Comparative Landscape of Small RNAs in Tissue and Liquid Biopsies for Liver Transplant Outcomes

Monima Anam[1], Christine Watkins[2], Grace Rucker[2], Katherine Marlow[1], Matthew Khalil[2], Murat Dogan[2], James Eason [2,3,4], Jason Vanatta [2,3], Corey Eymard [2,3], Cem Kuscu[2], Zhangli Su*[1], Canan Kuscu*[2]

[1] Department of Genetics, University of Alabama at Birmingham, Birmingham, AL, 35233, United States

[2] Transplant Research Institute, Department of Surgery, University of Tennessee Health Science Center, Memphis, TN, 38163, United States

[3] Methodist University Hospital, Memphis, TN, 38163, United States

[4] Current address: HCA Florida Hospitals, Largo, FL, 33770, United States

*Correspondence: Canan Kuscu (ckuscu@uthsc.edu) and Zhangli Su (zsu@uab.edu)

Abstract:

Background:

Ischemia-reperfusion injury (IRI) is an inevitable consequence of liver transplantation, arising during donor organ procurement and reoxygenation. Severe IRI is a leading contributor to early allograft dysfunction (EAD), a post-transplant complication associated with reduced graft survival. Current postoperative biomarkers provide limited time for intervention, highlighting a need to identify preoperative biomarkers of IRI. Meanwhile,

tRNA fragments (tRFs) have emerged as novel biomarkers in various diseases but remain unexplored in the context of liver transplant.

Results:

We performed small RNA sequencing on 96 paired donor liver biopsies from 48 patients to investigate IRI-associated transcript changes. In parallel, 161 donor liver perfusates were analyzed as a non-invasive surrogate for tissue. Across samples, microRNAs (miRNAs) and tRFs were the most abundant. Perfusate expression strongly correlated with biopsies, supporting their value as a non-invasive source of small RNAs. Comparison between post-reperfusion and pre-implantation biopsies revealed that IRI reprogrammed tRF expression. Stratification by clinical outcome showed that patients who developed EAD exhibited specific small RNA signatures in both biopsy and perfusate. Receiver operating characteristic (ROC) analysis revealed a miRNA-based model that achieved an AUC of 0.772, outperforming donor risk index alone (AUC = 0.665), representing a 10.7% increase in discriminative capacity.

Conclusions:

These results are the first to establish tRFs as IRI-responsive biomolecules abundant in both donor liver tissue and non-invasive perfusate. In particular, various small RNAs emerged as promising candidate biomarkers for early detection of EAD. These results lay the foundation to further investigate the prognostic utility of tRFs/miRNAs in liver transplantation.

Keywords (3-10):

tRFs, miRNAs, non-invasive biomarkers, ischemia-reperfusion injury, early allograft dysfunction, liver transplantation

Background

Ischemia-reperfusion injury (IRI) is an inevitable consequence of solid organ transplantation, initiated during donor organ procurement and cold storage, and exacerbated upon reperfusion in the recipient. The sudden reoxygenation of ischemic tissue induces a complex interplay of oxidative stress, metabolic disturbances, sterile inflammation, and cell death pathways that impair graft integrity (1). Severe IRI is a principal contributor to early allograft dysfunction (EAD), a clinical syndrome presenting within the first week post liver transplant, associated with increased morbidity, primary nonfunction, and diminished long-term graft survival (2). Current diagnostic criteria for EAD primarily rely on postoperative serum biochemical markers such as alanine aminotransferase (ALT) and aspartate aminotransferase (AST), which provide limited mechanistic insight and insufficient lead time for intervention (3). This underscores the need for high-resolution molecular biomarkers capable of detecting early transcriptional and post-transcriptional responses to IRI in graft tissue and accessible biofluids, thereby enabling predictive and mechanism-informed monitoring after liver transplantation.

Small RNAs are central regulators of post-transcriptional gene expression, modulating mRNA stability, translation, and chromatin organization across diverse biological contexts. Beyond well-characterized microRNAs (miRNAs) and piRNAs, transfer RNA-derived fragments (tRFs) and stress-induced tRNA halves (tiRs) have recently emerged as abundant and functionally versatile small RNA species generated by precise cleavage of precursor or mature tRNAs (4). Their biogenesis is strongly induced by cellular stressors, including oxidative injury, nutrient deprivation, hypoxia, and immune activation (5,6). Functionally, tRFs repress global protein synthesis, promote

74 stress granule assembly, displace messenger RNAs from RNA-binding proteins such as
75 YBX1, and participate in RNA silencing pathways via Argonaute association (7–10). A
76 recent publication also demonstrated that hypoxia induced tRF promotes cellular
77 homeostasis and protects against kidney injury by enhancing autophagic flux (11).
78 Through these mechanisms, tRFs act as dynamic modulators of cellular adaptation to
79 stress, influencing survival, metabolism, and signaling, positioning them as promising
80 molecular sentinels of stress phenotypes in both experimental and clinical settings (12,13).
81 Recent advances in transcriptomic profiling have identified small RNA signatures
82 as a promising class of molecular biomarkers for disease diagnosis, prognosis, and
83 therapeutic monitoring. Their inherent stability in biofluids, resistance to RNase
84 degradation, and ability to reflect dynamic physiological states make them well-suited for
85 minimally invasive diagnostics (14,15). miRNAs have been explored as potential
86 biomarkers in kidney and liver transplant (16–18). In liver transplantation, liver-specific
87 miR-122 detected in recipient serum was shown to be correlated with ALT and AST levels,
88 thus IRI severity and EAD (19). Furthermore, donor organ preservation solution
89 (perfusate) has emerged as an attractive biospecimen for biomarker discovery, capturing
90 molecules released directly from the donor liver during storage and perfusion (20,21).
91 While these investigations provide important proof-of-concepts, they focused on targeted
92 RNA species rather than unbiased transcriptome-wide profiling. Consequently, the
93 broader RNA repertoire within perfusate, including stress-responsive small RNAs such
94 as tRFs and tiRs, remains largely unexplored. Here, we report the first transcriptome-wide
95 small RNA profiling of 96 paired liver transplant biopsies from 48 patients alongside

96 perfusate samples from 161 donor organs, aimed at uncovering mechanistically linked
97 early non-invasive biomarkers of graft function that complement tissue-based assays.
98
99 **Results**
100 **Small RNAs and tRFs are abundantly expressed in donor liver transplant biopsy**
101 **samples.**
102 To characterize small RNAs present in donor liver tissue and determine whether
103 they change from pre- to post-transplantation, we collected paired donor liver biopsy
104 samples (n = 48) at two timepoints: pre-implantation (L1) and post-reperfusion (L2),
105 followed by small RNA sequencing analysis (**Fig. 1A**). Principal component analysis (PCA)
106 of all 96 samples revealed distinct separation between L1 and L2 small RNA expression
107 profiles, with PC1 and PC2 accounting for 19% and 12% of the variance, respectively
108 (**Fig. 1B).** A variety of small RNA species were detected through sequencing; however,
109 miRNAs comprised the largest proportion of mapped reads, followed by tRFs (**Fig. 1C**).
110 Four tRF subtypes dominated the tRF landscape: tiR5, tRF5, tRF3CCA, and tRF1 species
111 (**Fig. 1D and E**). tiR5s are known as 5' tRNA halves, which are typically 30–35 nucleotides
112 (nt) in length, while tRF5s are shorter 5' tRNA fragments that range from 15–29 nt long.
113 tRF3CCAs are 3' tRNA fragments that retain 3' CCA tails, a feature of mature tRNAs.
114 While tRF1s are the remnant 3' trailer sequences that are cleaved from precursor tRNAs
115 to form mature tRNAs. These four tRF subtypes represented the majority of mapped tRF
116 reads across samples. Additionally, tRFs derived from Glu- and Gly-carrying parental
117 tRNAs were highly enriched relative to other amino acid isotypes (**Fig. S1A**). Furthermore,
118 multiple specific tRF species rivaled the expression of the topmost expressed miRNAs,

119 such as Glu CTC tiR5 and Gly GCC tiR5, which were the fourth- and sixth-most highly
120 expressed small RNAs across samples (**Fig. S1A-B**). Overall, we observe that tRFs are
121 steadily abundant across L1 and L2 samples, serving as promising candidates for further
122 investigation.
123
124 **Comparison of L2 vs. L1 expression profiles reveals IRI-associated tRF changes.**
125 We next examined small RNAs differentially expressed in response to IRI by
126 comparing L2 and L1 samples, as L2 samples were collected post-reperfusion and
127 therefore serve as a proxy for transplant-associated IRI. DESeq2 analysis of paired L2
128 vs. L1 small RNA profiles revealed 182 differentially expressed small RNAs, including 116
129 tRFs and 66 miRNAs (**Supplementary Table 1**). Of these, 102 (58 tRFs, 44 miRNAs)
130 were upregulated and 80 (58 tRFs, 22 miRNAs) were downregulated in L2 compared to
131 L1 (**Fig. 2A and B**). Strikingly, tRFs of the same subtype displayed uniform directional
132 changes. Among the most abundant tRF classes, differentially expressed tiR5s were
133 consistently enriched in L2, while significant tRF3CCA species were consistently depleted
134 in L2. Similar trends were observed for differentially expressed tRF1 and tRF5 species,
135 with the majority showing upregulation following IRI (**Fig. 2B**). Boxplots of select tiR5 and
136 tRF3CCA species likewise exemplify and highlight this trend (**Fig. 2C-E**). Together, these
137 findings indicate that IRI is associated with subtype-specific changes in tRF expression,
138 suggesting that tRF dysregulation may be a characteristic feature of IRI.
139
140 **IRI-associated tRF changes are stratified by transplant outcome.**

141 Next, we stratified patients by early transplant outcome to assess whether IRI-
142 associated tRF changes were uniquely associated with graft dysfunction. Transplant
143 outcomes were based on day 1 AST values (2), where high AST values (>2000)
144 corresponded to early allograft dysfunction (EAD, n = 18) and moderate/low AST values
145 corresponded to normal function (NF, n = 30) **(Fig. 3A and S2A)**. DESeq2 analysis of L2
146 vs. L1 in each outcome group (EAD or NF) revealed group-dependent regulation of tRFs.
147 In the EAD group, L2 biopsies showed unique upregulation of numerous tiR5 species not
148 observed in NF samples **(Fig. 3B and C)**. In contrast, the NF group exhibited unique
149 upregulation of multiple tRF1 species in L2 vs. L1 comparisons **(Fig. 3B, S2C and D)**.
150 Notably, no tiR5 species were downregulated in L2 in either group **(Fig. S2E)**.
151 Downregulated RNAs in L2 were largely shared between groups and consisted primarily
152 of tRF3CCA species **(Fig. S2E and F)**. The complete comparison is also included in
153 **Supplementary Table 1.** Overall, we observe that post-IRI tRF changes are uniquely
154 dysregulated in EAD and NF grafts, suggesting that tRFs may be prognostically linked to
155 graft outcome.
156

157 **Comparison of EAD vs. NF small RNA profiles reveals transplant outcome-**
158 **associated small RNA changes, independent of IRI.**

159 To evaluate whether small RNA profiles differed between EAD and NF grafts, we
160 performed differential expression analysis (EAD vs. NF) separately within L1 and L2
161 samples, including batch correction. This approach allowed us to identify small RNAs
162 associated with transplant outcome independent of IRI-induced changes. DESeq2
163 analysis revealed multiple differentially expressed small RNAs that were shared across

164 EAD vs. NF comparisons (**Supplementary Table 2**). Specifically, miR-452-5p, miR-224-
165 5p, and miR-296-3p were significantly upregulated in EAD samples compared to NF
166 samples (**Fig. 4A–E and Fig. S3A**). In contrast, two small RNAs were consistently
167 downregulated in EAD, including Gly TCC tRF3CCA and miR-1247-5p (**Fig. S3B**). To
168 understand potential biological functions of EAD-associated miRNAs, we performed
169 pathway enrichment analysis of predicted mRNA targets of the three miRNAs consistently
170 upregulated in EAD samples. Network analysis revealed that miR-224-5p, miR-452-5p,
171 and miR-296-3p share overlapping target gene networks (**Fig. 4F**). Reactome pathway
172 enrichment analysis of these miRNA targets identified significant enrichment of pathways
173 related to cellular stress response, various signaling pathways (SCF-KIT, ERBB4, FCERI),
174 and chromatin organization and modification (**Fig. 4F**). Notably, the most significantly
175 enriched pathway was "cellular response to stress" (FDR = 0.000286), suggesting that
176 dysregulation of stress pathways may underlie the association between these miRNAs
177 and EAD. No significant pathways were identified for the two small RNAs (Gly TCC
178 tRF3CCA and miR-1247-5p) consistently downregulated in EAD samples. Together,
179 these findings demonstrate that small RNA profiles differ between EAD and NF groups,
180 regardless of IRI status, suggesting that pre-implantation profiles may be sufficiently
181 informative to aid in predicting EAD.
182
183 **Pre-transplant liver perfusate is enriched with tRFs and small RNA species.**
184 To determine whether liver biopsy-associated tRF and miRNA changes could be
185 captured non-invasively, we analyzed small RNAs in donor liver preservation solution
186 (now referred to as perfusate). Donor livers were submerged in preservation solution and

187 transported on ice prior to transplantation. Immediately before implantation, perfusate
188 was collected and analyzed based on EAD (n = 49) and NF (n = 112) presence (**Fig.**
189 **S4A**). RNA was extracted from the perfusate and a robust signal corresponding to small
190 RNA size was detected after library construction (**Fig. 5A and Fig. S4B**). The size
191 distribution from the perfusate appears different from the one derived from tissue,
192 highlighting specific enrichment of small RNAs in the perfusate (**Fig. S4B**). As a readily
193 accessible biofluid that does not require tissue biopsy, liver perfusate represents a
194 promising non-invasive source for biomarker discovery. Small RNA sequencing revealed
195 a high abundance of small RNAs in perfusate, with tRFs as the most prevalent class,
196 followed by mitochondrial tRFs (MtRFs) (**Fig. 5B**). Comparisons between perfusates from
197 EAD versus NF donors showed no significant differences in the overall distribution of
198 small RNA classes; tRFs and miRNAs were similarly abundant across both groups (**Fig.**
199 **5C).** Pearson correlations revealed moderate to strong relationships between perfusate
200 and both L1 (mean R = 0.70) and L2 (mean R = 0.72) tissue profiles (**Fig. S5A and S5B**),
201 indicating that perfusate partially recapitulates the tissue molecular landscape. Despite
202 the lack of global differences, the consistently high levels of tRFs/miRNAs and other small
203 RNAs in perfusate highlight its potential as a platform for identifying novel RNA
204 biomarkers predictive of donor liver quality and transplant outcomes.
205

206 **Pre-transplant perfusate small RNAs are analogous to tissue profiles and are**
207 **differentially expressed in EAD.**

208 Given the variable level of tRFs/miRNAs across samples (**Fig. 5C**), we evaluated whether
209 perfusate small RNA composition correlated with donor clinical variables, starting with the

210 donor risk index (DRI), a composite metric that incorporates donor age, cold ischemia
211 time, cause of death, and race (22). We observed that miRNA percentage was
212 significantly positively correlated with DRI (**Fig. 6A**). Similarly, tRF percentage was
213 significancy negatively correlated with DRI (**Fig. 6B**). These correlations suggest that DRI
214 is associated with the overall perfusate small RNA composition. Examination of the
215 individual DRI components indicated that cause of death was the primary contributor to
216 this association (**Fig. S5C**). We next investigated whether pre-transplant perfusate small
217 RNAs could reflect donor liver quality independent from known clinical variables and
218 serve as potential biomarkers for EAD. To do this, we performed differential expression
219 analysis comparing EAD vs. NF groups using DESeq2 with correction for batch and donor
220 risk index (22). Multiple small RNA species showed differential expression in EAD (**Fig.
221 6C and D, Supplementary Table 2**), suggesting these small RNAs could be potential
222 predictors of EAD independent of donor clinical information. Notably, multiple differentially
223 expressed small RNAs were among the top fifty most highly expressed small RNAs in
224 perfusate samples (**Fig. 6E**). These include Gly GCC/CCC tiR5, Glu CTC/TTC tiR5, Lys
225 CTT tiR5, and miR-26a-5p, all of which were increased in EAD samples, as well as let-
226 7b-5p, which was decreased in EAD samples. Collectively, these findings demonstrate
227 that pre-transplant liver perfusate can serve as a non-invasive source of small RNAs that
228 partially reflect donor liver tissue profiles. The presence and differential expression of
229 perfusate-derived small RNAs further support their potential utility as non-invasive
230 biomarkers for predicting EAD.
231

232 **EAD-downregulated perfusate miRNAs improve prediction of early allograft**
233 **dysfunction.**

234 To evaluate whether perfusate small RNAs differentially expressed between EAD and NF
235 could serve as predictive biomarkers, we performed 5-fold cross-validated ROC analyses
236 using multiple feature sets derived from DESeq2 results using 155 patients with available
237 clinical parameters. Predictive performance was compared against using DRI alone.
238 Models incorporating EAD-upregulated perfusate small RNAs did not outperform DRI
239 alone (AUC = 0.665; 95% CI, 0.576–0.754). Notably, upregulated miRNAs performed
240 poorly both alone and in combination with DRI (AUC = 0.596; 95% CI, 0.490–0.701; **Fig.**
241 **S5D**). In contrast, models based on EAD-downregulated perfusate small RNAs
242 demonstrated improved discriminatory capacity. A combined set of downregulated
243 miRNAs and tRFs achieved an AUC of 0.756 (95% CI, 0.668–0.844) alone and 0.764
244 (95% CI, 0.677–0.851) when combined with DRI (**Fig. 7A**). Stratification by small RNA
245 class revealed that this improvement was driven primarily by miRNAs. Downregulated
246 perfusate miRNAs alone achieved an AUC of 0.762 (95% CI, 0.675–0.850), which further
247 increased to 0.772 (95% CI, 0.686–0.859) when combined with DRI, representing an 10.7%
248 improvement over DRI alone (**Fig. 7B**). DeLong's test revealed no significant difference
249 between the miRNA-alone and DRI-alone models (p = 0.106), indicating comparable
250 predictive performance. In contrast, the combined miRNA + DRI model significantly
251 outperformed the DRI-only model (p = 0.033), demonstrating that the addition of these
252 miRNAs resulted in a significant improvement in discriminatory capacity.

253 This miRNA model comprised nine miRNAs (let-7b-5p, miR-128-2-3p, miR-223-
254 5p, miR-375-3p, miR-383-5p, miR-4448-3p, miR-486-3p, miR-499-5p, and miR-514a-1-

255 5p) significantly downregulated in EAD perfusate samples (**Fig. 7C**), six of which showed
256 negative correlations with post-transplant day 1 AST and/or ALT levels (**Fig. S6B**). In
257 contrast, downregulated perfusate tRFs did not improve predictive performance beyond
258 DRI (AUC = 0.648; 95% CI, 0.552–0.743) and failed to show significant correlations with
259 early post-transplant liver injury markers (**Fig. S6B and C**). To explore potential biological
260 mechanisms underlying these associations, we performed pathway enrichment analysis
261 of predicted mRNA targets of the nine EAD-downregulated perfusate miRNAs. Network
262 analysis demonstrated substantial overlap in target gene networks among these miRNAs
263 (**Fig. 7C**). Reactome pathway enrichment analysis identified significant enrichment of
264 multiple signaling pathways, including SOS-mediated signaling, FCERI, EGFR, leptin,
265 RAF/MAP kinase, and SCF-KIT signaling pathways (**Fig. 7D and Supplementary Table**
266 **3**). Notably, "cellular responses to stress" re-emerged as the most significantly enriched
267 pathway (FDR = 6.08×10^{-8}), consistent with findings from tissue-based EAD versus NF
268 comparisons (**Fig. 4F** and **Fig. 7D**), while "SOS-mediated signaling" was the second most
269 significantly enriched pathway (FDR = 2.68×10^{-7}). Together, these results demonstrate
270 that EAD-downregulated perfusate miRNAs could serve as predictive biomarkers for early
271 allograft dysfunction independent from established clinical risk metrics. Importantly, these
272 miRNAs can be non-invasively measured in pre-transplant perfusate, highlighting their
273 potential utility for enhancing donor risk stratification prior to transplantation.
274

275 **Discussion**

276 In this study, we performed small RNA sequencing on donor liver biopsies from 48
277 cases and reported abundant tRFs (**Fig. 1**). Analysis of paired post-reperfusion versus

278 pre-implantation biopsies revealed that ischemia-reperfusion injury increased tiR5 and
279 tRF1 species, alongside a decrease in tRF3CCA (**Fig. 2**). Notably, tiR5 was particularly
280 enriched in post-reperfusion L2 tissues from patients who developed EAD, whereas tRF1
281 upregulation was specific to those with NF graft outcomes (**Fig. 3**). In parallel, comparison
282 of EAD vs NF in L1 and L2 independently highlighted miRNAs and tRFs which are
283 important for EAD pathology (**Fig. 4**). As a proof of concept to use organ preservation
284 solution (perfusate) for non-invasive biomarker discovery, we sequenced perfusate small
285 RNAs from 161 samples and observed abundant tRFs and miRNAs that are likely derived
286 from liver tissues (**Fig. 5**). Comparison of perfusate small RNAs in patients with EAD
287 versus NF identified multiple differentially expressed small RNAs including tRFs and
288 miRNAs (**Fig. 6**). Importantly, a set of nine downregulated perfusate miRNAs can predict
289 post-transplant outcome more effectively than using donor clinical information alone (**Fig.**
290 **7**). Our integrated analysis of liver biopsies and perfusate revealed that both
291 compartments contain a shared repertoire of small RNAs, highlighting the potential utility
292 of these small RNAs as non-invasive biomarkers for IRI and post-transplant outcomes.

293 The observed increase of multiple tiR5 species in L2 (**Fig. 2B-D**) is likely due to
294 the hypoxia and oxidative stress incurred during static cold storage and reperfusion,
295 consistent with the well-established role of tiR5s as stress-induced RNAs, including in
296 hypoxic contexts (4,13). During cellular stress, these tiR5s have been shown to bind to
297 translation initiation factors such as eIF4G/A and displace the eIF4F complex from
298 mRNAs, resulting in global suppression of protein synthesis while permitting selective
299 translation of stress-adaptive transcripts (23). In addition, tiR5s facilitate the assembly of
300 stress granules, sequestering non-essential mRNAs to further conserve resources and

301 prioritize production of proteins critical for survival and recovery (8). Beyond stress
302 adaptation, infection-induced tiR5s have also been implicated in immune activation,
303 particularly through Toll-like receptor 7 interaction (24–26). Given that IRI is characterized
304 as a sterile inflammatory process in which innate immunity plays a central role, the
305 observed tiR5 induction may represent a mechanistic link between cellular stress and
306 immune activation. In particular, the greater tiR5 increase in patients who developed EAD
307 (**Fig. 3B-C**) could indicate more tissue damage or immune activation in those transplants.
308 Conversely, the specific increase in tRF1s upon reperfusion in patients with NF (**Fig. 3B**
309 **and Fig. S2D**) raises the possibility of a protective role for tRF1 that warrants further
310 mechanistic exploration. Future investigation to identify the molecular targets of these
311 clinically relevant liver tRFs will be needed to reveal their biological functions in the
312 context of IRI stress and organ transplantation (**Fig. 8A**).

313 Comparisons of EAD versus NF samples in both L1 and L2 tissue cohorts
314 independently identified upregulated miRNAs, including miR-452-5p, miR-224-5p, and
315 miR-296-3p (**Fig. 4A–E**). Target-gene enrichment analysis showed that these miRNAs
316 converge on SOS-mediated and stress-response pathways (**Fig. 4F–G**). Functionally,
317 miR-452-5p has been shown to promote proliferation and cell-cycle progression in
318 hepatocellular carcinoma (27), suggesting a potential role in supporting regenerative
319 responses following injury. Similarly, E2F1-driven induction of miR-224-5p is required for
320 liver cancer progression and invasion (28), indicating that miR-224-5p may enhance cell
321 survival under stress. In contrast, miR-296-3p has been reported to attenuate liver fibrosis
322 (29). Together, these observations suggest a coordinated response in EAD patients in

323 which miR-452-5p and miR-224-5p may promote proliferation and regeneration, while
324 miR-296-3p may contribute to fibrosis suppression and injury resolution (**Fig. 8B**).

325 The identification of tRFs as dominant small RNAs in perfusate is particularly
326 exciting and demonstrates their potential for use in liquid biopsy monitoring (**Fig. 5**). This
327 is particularly important for evaluating marginal organs and machine perfusion settings,
328 where clinically validated, predictive molecular markers are still lacking. Previously,
329 Verhoeven et al. identified mRNAs and microRNAs in graft preservation solution
330 (perfusate) correlating with early injury (20), while Matton et al. reported that miRNA
331 profiles in normothermic perfusion solution could inform liver viability assessments (21).
332 Both studies were limited to targeted approaches. Darden et al. recently compared
333 miRNA profiles across donor types and recipient outcomes using liver preservation
334 solution and identified distinct miRNA signatures for each donor category, although the
335 study was limited by a small patient cohort (30). Our application of unbiased, next-
336 generation sequencing to perfusate along with tissue small RNA profiling identified
337 clinically relevant miRNAs and tRFs (**Fig. 6 and Fig 7**).

338 Intriguingly, the set of downregulated miRNAs that enhance EAD prediction (let-
339 7b-5p, miR-128-2-3p, miR-223-5p, miR-375-3p, miR-383-5p, miR-4448-3p, miR-486-3p,
340 miR-499-5p, and miR-514a-1-5p) is enriched in SOS-mediated and broader cellular
341 stress-response pathways (**Fig. 7 and Fig. 8C**). SOS functions as a key upstream
342 activator of Ras proteins, initiating the canonical Ras/Raf/MEK/ERK signaling cascade.
343 This pathway plays a crucial role in promoting the proliferation and survival of hepatocytes
344 and hepatic stellate cells, particularly during cellular stress and liver regeneration (31).
345 Among these miRNAs, let-7b-5p and miR-514a-5p are well-characterized tumor

346 suppressors in hepatocellular carcinoma (32,33). Their reduced expression in EAD may
347 relieve inhibitory constraints on hepatocyte proliferation, thereby supporting early survival
348 responses following graft injury. Furthermore, previous experimental studies have shown
349 that inhibition of miR-128-3p attenuates liver ischemia–reperfusion injury in mice (34),
350 which is consistent with our observation that miR-128-3p is also downregulated in EAD
351 patients. Together, these findings suggest that clinically relevant stress-responsive
352 miRNAs may actively modulate hepatocyte survival pathways during early allograft injury.
353 Targeting or modulating these miRNAs could represent a promising strategy to enhance
354 cellular recovery and improve postoperative outcomes in EAD (**Fig. 8**). In addition,
355 although these small RNAs predict the initial post-transplant outcome, their roles and
356 potential influence in long-term clinical trajectories such as rejection and overall graft
357 lifespan requires further investigation.

358 Studies of this kind will ultimately enable the transplant community to identify
359 robust small RNA–based biomarkers and accelerate the development of practical
360 detection platforms for real-world application. qPCR-based miRNA and tRF panels, for
361 example, could be implemented during organ procurement or machine perfusion to
362 support rapid, on-site assessment of graft quality. In parallel, emerging CRISPR-based
363 RNA detection technologies, such as the Cas13-driven SHERLOCK system (35), offer
364 highly sensitive, rapid, and field applicable alternatives that could further strengthen
365 intraoperative decision making. Moreover, recent advances in serum and plasma small
366 RNA detection for cancer associated miRNAs (36,37) provide a strong technical
367 foundation that is readily translatable to organ transplantation workflows.

368 While these opportunities are compelling, several technical considerations
369 inherent to small RNA sequencing must be acknowledged. Small RNA-seq library
370 preparation is prone to sequence-specific biases, including differences in adapter ligation
371 efficiency, GC content, and secondary structure, which can lead to over- or under-
372 representation of certain small RNA species. These biases, however, are well described
373 and can be minimized through standardized protocols and appropriate normalization
374 strategies, both of which were applied in our analysis. Although variation in sequencing
375 depth can affect detection of very low-abundance miRNAs, the depth achieved here was
376 sufficient to reliably characterize the predominant small RNA populations in all sample
377 types. Due to limited RNA availability, particularly in perfusate samples, we were unable
378 to perform additional qPCR validation, and therefore our findings rely on sequencing-
379 derived quantification alone. As such, while the identified small RNA signatures are
380 biologically plausible and reinforced by pathway-level analyses, they should be validated
381 in future studies using independent cohorts and targeted assays.
382

383 **Conclusion**

384 Despite the technical limitations, this study provides the first transcriptome-wide
385 characterization of small RNAs in both human liver tissue and donor organ perfusate
386 during transplantation. We demonstrate that specific tRFs and miRNAs are closely linked
387 to reperfusion and EAD. The prevalence of tRFs and miRNAs in perfusate highlights their
388 potential as non-invasive biomarkers, bridging molecular insights from tissue with
389 clinically accessible diagnostics. By uncovering both shared and compartment-specific
390 signatures, our findings lay a foundation for future validation in larger cohorts and under

391 machine perfusion, advancing systems-level small RNAs toward clinical application for
392 improved pre-operative organ assessment and peri-operative transplant monitoring.

393

394

Figures and Figure Legends

Figure 1

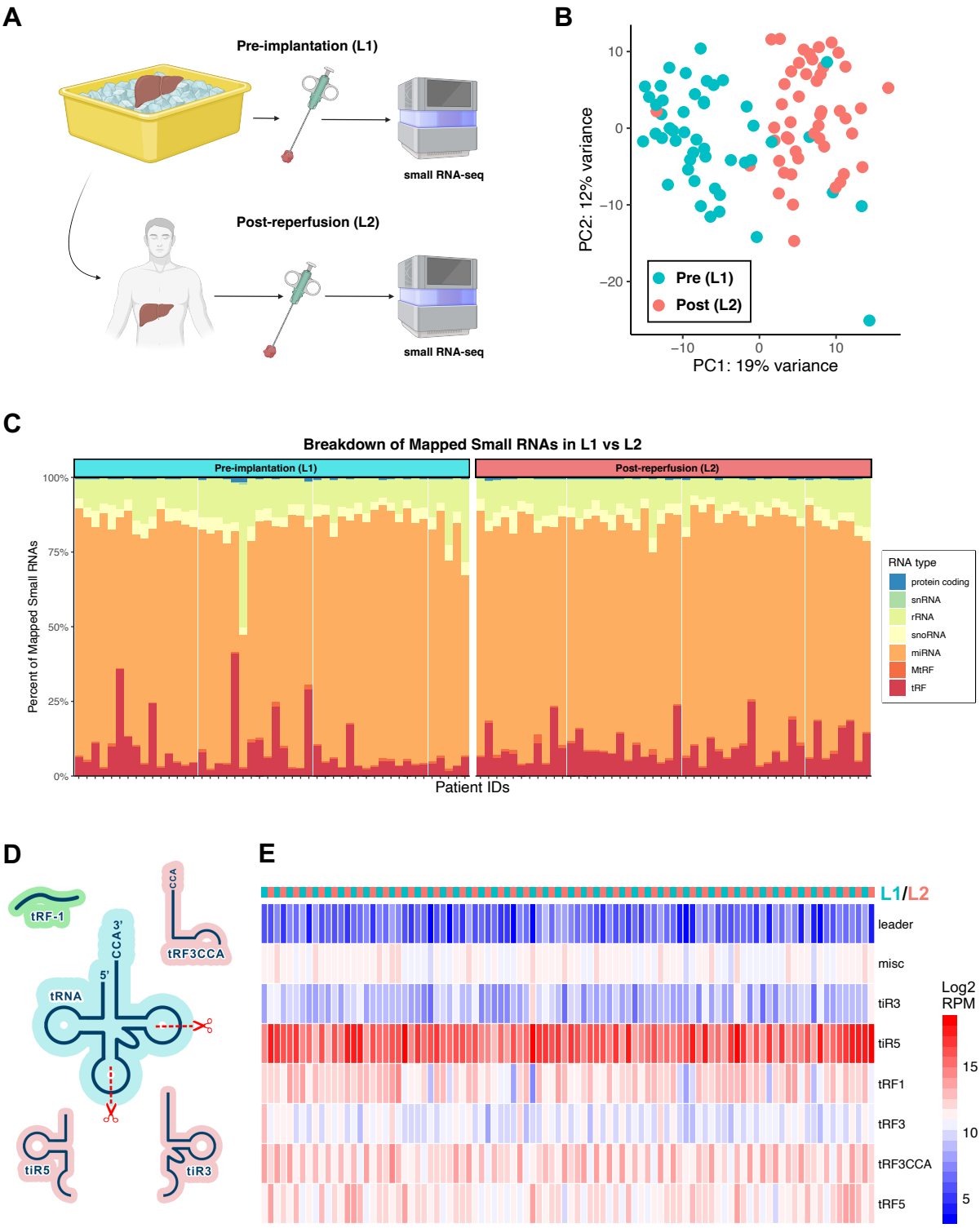

398 **Figure 1. Abundance of tRNA fragments (tRFs) in 96 donor liver transplant biopsy**
399 **samples.**
400 **(A)** Paired liver biopsy samples were obtained from donor livers at two time points: pre-
401 implantation (L1, n = 48) and post-reperfusion (L2, n = 48), followed by small RNA
402 sequencing. **(B)** Principal component analysis (PCA) of small RNA sequencing data
403 reveals distinct clustering between L1 and L2 small RNA profiles. **(C)** Stacked bar plot
404 displaying the proportion of mapped reads for each small RNA type in L1 and L2 samples.
405 For each patient (x-axis), the bars represent the relative proportion of total reads (y-axis)
406 assigned to each small RNA type. Across samples, miRNAs comprised the largest
407 majority of mapped reads, followed by tRFs. **(D)** Schematic illustrating four highlighted
408 tRF subtypes. The tRF nomenclature echoes the region of tRNA from which tRFs are
409 derived. The fragments shown are examples of each tRF subtype and do not represent
410 all possible variants. tRF-1 species (green) are derived from precursor tRNAs (not
411 pictured), while tiR5, tiR3, and tRF3CCA species (pink) are cleaved from mature tRNAs
412 (blue). **(E)** Heatmap displaying the relative expression (Log2 RPM) of different tRF
413 subtypes across L1 and L2 samples. Overall, biopsy samples showed abundant tRF
414 expression.
415
416

417

Figure 2

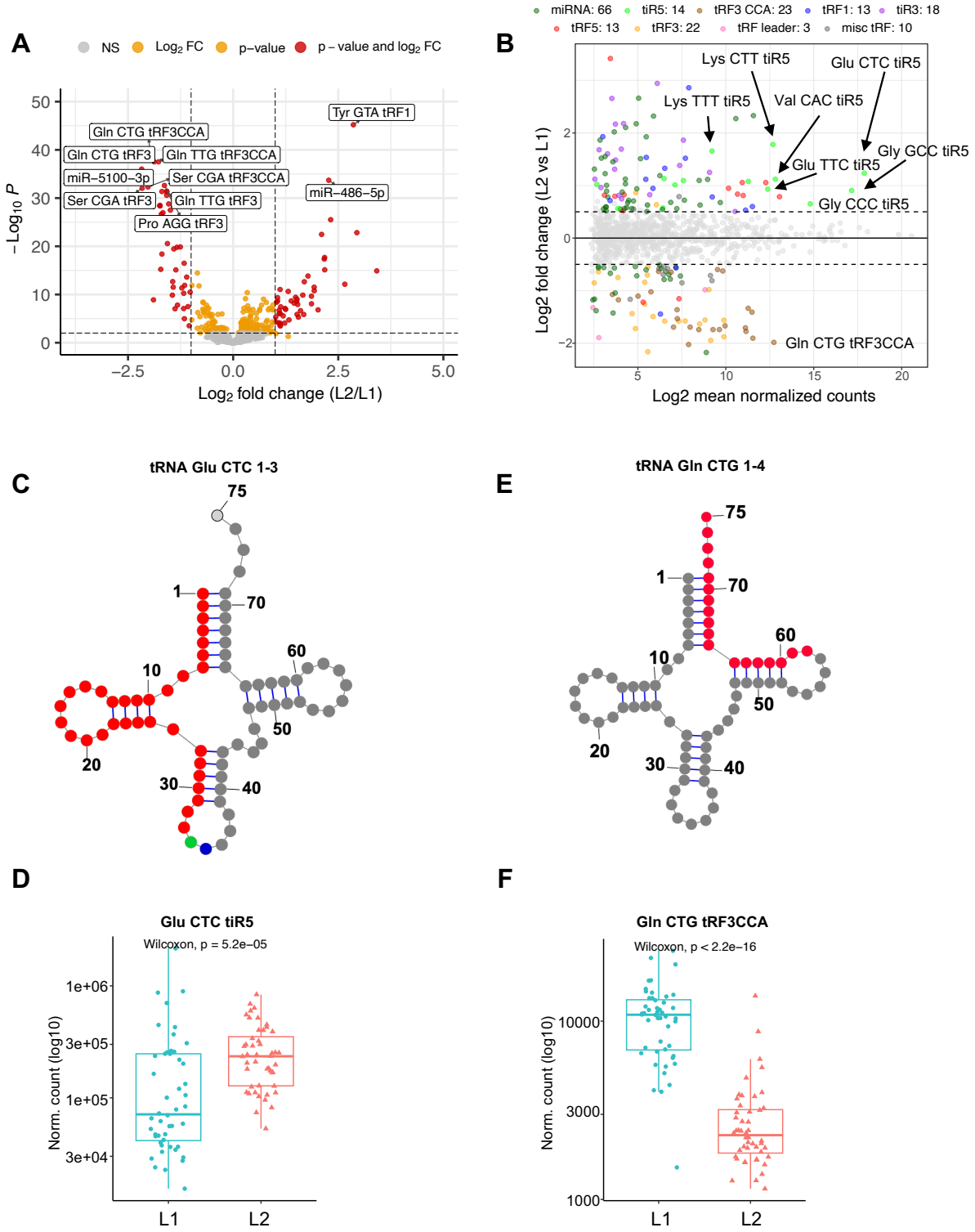
A
NS
Log2 FC
p-value
p - value and log2 FC
Tyr GTA tRF1
Gln CTG tRF3CCA
Gln CTG tRF3
Gln TTG tRF3CCA
miR-5100-3p
Ser CGA tRF3CCA
Ser CGA tRF3
Gln TTG tRF3
miR-486-5p
Pro AGG tRF3
-Log10 P
Log2 fold change (L2/L1)
B
miRNA: 66
tiR5: 14
tRF3 CCA: 23
tRF1: 13
tiR3: 18
tRF5: 13
tRF3: 22
tRF leader: 3
misc tRF: 10
Lys CTT tiR5
Glu CTC tiR5
Lys TTT tiR5
Val CAC tiR5
Gly GCC tiR5
Glu TTC tiR5
Gly CCC tiR5
Gln CTG tRF3CCA
Log2 fold change (L2 vs L1)
Log2 mean normalized counts
C
tRNA Glu CTC 1-3
E
tRNA Gln CTG 1-4
D
Glu CTC tiR5
Wilcoxon, p = 5.2e-05
Norm. count (log10)
L1
L2
F
Gln CTG tRF3CCA
Wilcoxon, p < 2.2e-16
Norm. count (log10)
L1
L2

418 **Figure 2. Significant tRF alterations associated with ischemia-reperfusion injury**
419 **(IRI) during liver transplantation.**
420 **(A)** Volcano plot of differentially expressed small RNAs between paired L2 and L1
421 samples, identified using DESeq2. The x-axis shows the log2 fold change (L2 vs. L1),
422 and the y-axis shows statistical significance (-log10 adjusted p-value). The top 10 most
423 significantly altered small RNAs are labeled, many being tRF3CCA species
424 downregulated in L2. **(B)** MA plot of differentially expressed small RNAs (L2 vs. L1)
425 identified using DESeq2 (p. adj < 0.05, |Log2FoldChange| > 0.5). The x-axis represents
426 gene expression (log2 normalized counts), and the y-axis shows the log2 fold change.
427 Differentially expressed RNAs are color-coded by RNA type (tRF subtype or miRNA).
428 Select highly abundant, significantly altered tRFs are labeled, including many tiR5 species
429 that are upregulated in L2. **(C)** Primary and secondary structure of parental tRNA-Glu-
430 CTC-1-3, with its most abundant tiR5 fragment highlighted in red (positions 1-35).
431 Cleavage sites that generate the second and third most abundant Glu CTC tiR5 isoforms
432 from tRNA-Glu-CTC are marked in green and blue. **D)** Boxplot of Glu CTC tiR5 expression
433 in L1 (n = 48) vs. L2 (n = 48) samples, showing significant upregulation in L2, consistent
434 with IRI-associated induction. **(E)** Primary and secondary structure of parental tRNA-Gln-
435 CTG-1-4, with its corresponding tRF3CCA fragment highlighted in red (positions 58–75).
436 **(F)** Boxplot of Gln CTG tRF3CCA expression in L1 (n = 48) vs. L2 (n = 48) samples,
437 showing significant downregulation in L2, indicative of IRI-associated suppression.
438
439
440

441

Figure 3

A

L1/L2 Biopsy sample summary (n = 48)

Group	EAD	NF	p value
Number of patients	18	30	
Recipient mean age	57.3	56.6	N.S.
Recipient gender (F/M)	7/11	10/19	N.S.
Donor mean age	47.4	37.7	0.012 *
Donor gender (F/M)	9/9	16/14	N.S.
Mean CIT (hours)	4.89	4.34	N.S.
Mean AST (Day 1)	5472.8	1072.4	2.7e-04 ***
Mean ALT (Day 1)	1618.3	542.5	0.0015 **

B

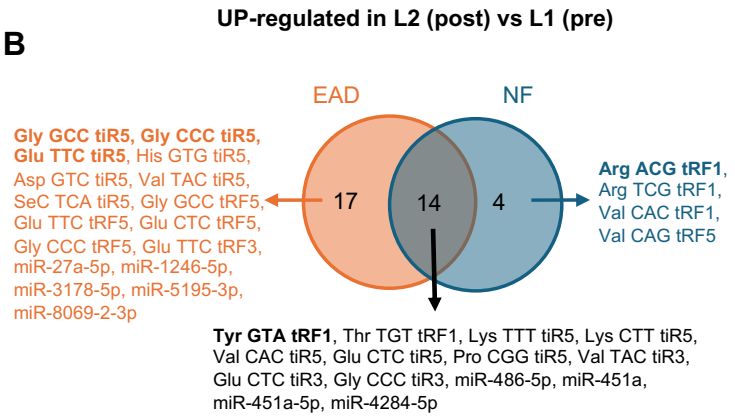

C

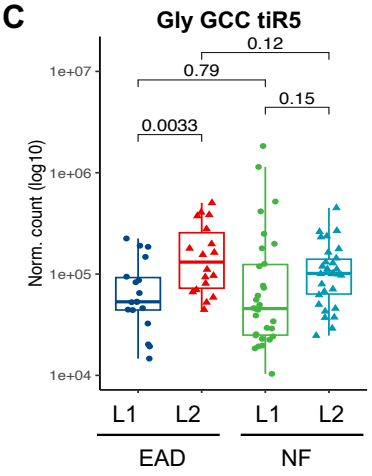

D

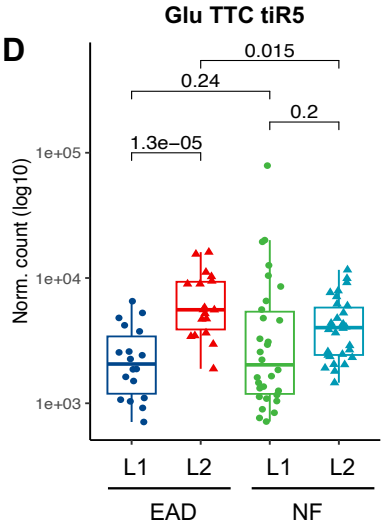

Figure 3. IRI-associated tRF alterations are transplant outcome specific.

(A) Clinical and demographic characteristics of the patient cohort, stratified by transplant outcome (EAD or NF), which was classified based on day 1 post-transplant aspartate aminotransferase (AST) levels. Cold ischemia time (CIT), the duration the donor liver remained on ice prior to transplantation, averaged 4.6 hours across groups. **(B)** Differential expression analysis of paired L2 vs. L1 samples was performed separately within EAD and NF groups (p. adj < 0.05). The Venn diagram displays small RNAs upregulated in L2 relative to L1 for each group. In the EAD group (n = 18), uniquely upregulated RNAs were predominantly tiR5 species, whereas in the NF group (n = 30), uniquely upregulated RNAs were mainly tRF1 species. A subset of tiR5 and tRF1 species was commonly upregulated in both groups, alongside other tRF and miRNA species. **(C)** and **(D)** Boxplots showing normalized expression (log10 transformed) of representative tiR5 species (Gly-GCC and Glu-TTC), stratified by transplant outcome (EAD vs. NF) and biopsy timepoint (L2 vs. L1). Statistical comparisons were performed using Wilcoxon rank-sum tests; p-values are indicated above comparisons. Both panels exemplify the EAD-specific upregulation of tiR5s, showing significant upregulation in L2 compared to L1 exclusively in EAD samples (Student's t-test).

465

Figure 4

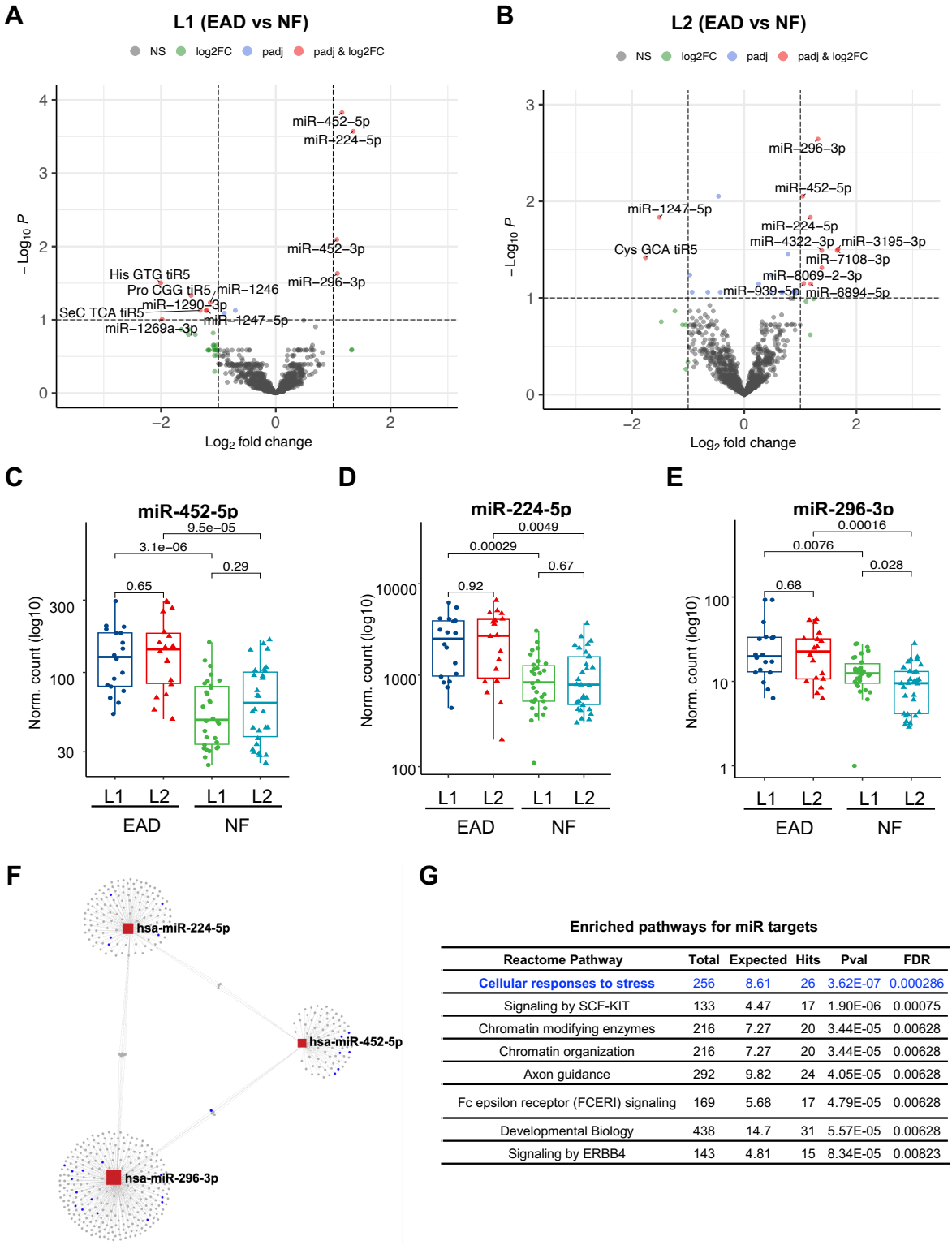

Enriched pathways for miR targets

Reactome Pathway	Total	Expected	Hits	Pval	FDR
Cellular responses to stress	256	8.61	26	3.62E-07	0.000286
Signaling by SCF-KIT	133	4.47	17	1.90E-06	0.00075
Chromatin modifying enzymes	216	7.27	20	3.44E-05	0.00628
Chromatin organization	216	7.27	20	3.44E-05	0.00628
Axon guidance	292	9.82	24	4.05E-05	0.00628
Fc epsilon receptor (FCERI) signaling	169	5.68	17	4.79E-05	0.00628
Developmental Biology	438	14.7	31	5.57E-05	0.00628
Signaling by ERBB4	143	4.81	15	8.34E-05	0.00823

466 **Figure 4. Transplant outcome-associated differences in liver biopsy small RNA**
467 **expression.**
468 **(A)** Volcano plot of differentially expressed small RNAs between early EAD and NF in L1
469 samples (n = 18 and 30 respectively), identified using DESeq2 (p. adj < 0.1). The x-axis
470 represents log2 fold change (EAD vs. NF), and the y-axis indicates statistical significance
471 (−log10 adjusted p-value). The topmost significantly altered small RNAs are labeled. **(B)**
472 Volcano plot of differentially expressed small RNAs between EAD and NF in L2 biopsy
473 samples (n = 18 and 30 respectively). The topmost significantly altered small RNAs are
474 labeled. **(C – E)** Boxplots of normalized expression (log10 transformed) of representative
475 miRNAs (miR-452-5p, miR-224-5p, miR-296-3p), stratified by transplant outcome (EAD
476 vs. NF) and biopsy timepoint (L1 vs. L2). All three miRNAs are consistently upregulated
477 in EAD compared to NF, independent of time point. Statistical comparisons were
478 performed using Wilcoxon rank-sum tests; p-values are shown above comparisons. **(F)**
479 The lefthand side shows a network visualization of the three differentially expressed
480 miRNAs, where red squares denote the miRNAs and surrounding circular nodes
481 represent their predicted mRNA targets. Target nodes highlighted in blue correspond to
482 genes belonging to the top enriched Reactome pathway, "Cellular responses to stress."
483 **(G)** The pathway enrichment results generated from the combined miRNA target set
484 (Reactome database, FDR cutoff = 0.01). For each pathway, the total number of
485 annotated genes, expected overlap, observed hits, p-value, and FDR-adjusted
486 significance are shown. "Cellular responses to stress" emerged as the most significantly
487 enriched pathway, consistent with the clustering of blue target nodes in the network plot.
488

489

Figure 5

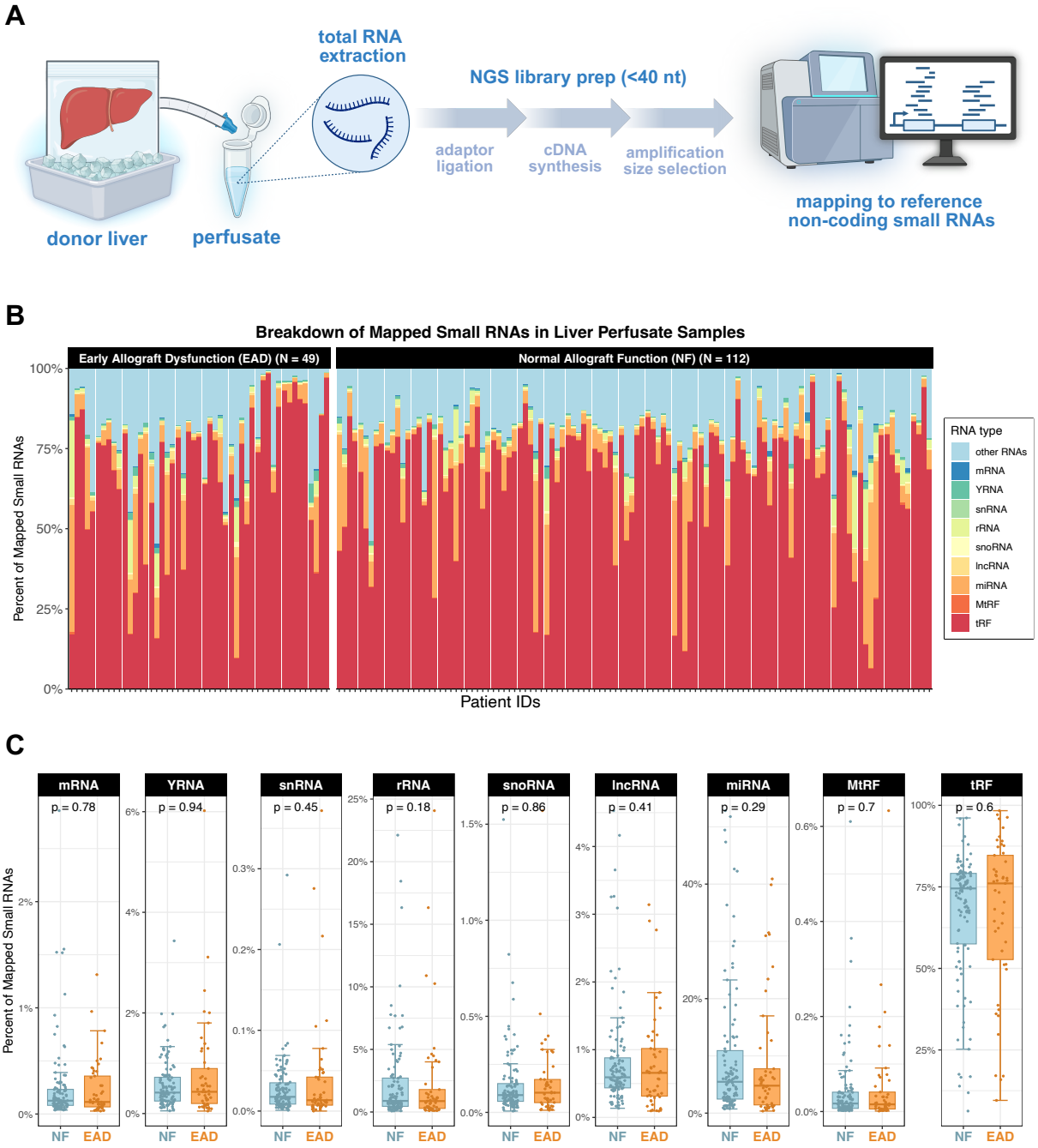
A
total RNA extraction
NGS library prep (<40 nt)
adaptor ligation
cDNA synthesis
amplification size selection
mapping to reference non-coding small RNAs
donor liver
perfusate
B
Breakdown of Mapped Small RNAs in Liver Perfusate Samples
Early Allograft Dysfunction (EAD) (N = 49)
Normal Allograft Function (NF) (N = 112)
Percent of Mapped Small RNAs
Patient IDs
RNA type
other RNAs
mRNA
YRNA
snRNA
rRNA
snoRNA
lncRNA
miRNA
MtRF
tRF
C
mRNA p = 0.78
YRNA p = 0.94
snRNA p = 0.45
rRNA p = 0.18
snoRNA p = 0.86
lncRNA p = 0.41
miRNA p = 0.29
MtRF p = 0.7
tRF p = 0.6
Percent of Mapped Small RNAs
NF
EAD

490 **Figure 5. Pre-transplant liver perfusate solution is enriched with small RNAs.**

491 **(A)** Donor livers were transported on ice in organ preservation solution prior to
492 transplantation. Immediately before transplantation, the preservation solution (perfusate)
493 was collected, and RNA was isolated for small RNA sequencing**. (B)** Composition of
494 mapped small RNAs in 161 liver perfusate samples, stratified by EAD and NF groups.
495 Across both groups, tRFs represented the predominant RNA species, followed by
496 mitochondrial tRFs (MtRFs). **(C)** Relative abundance of mapped small RNA classes in
497 liver perfusate samples, stratified by NF and EAD groups (n = 49 and 112 respectively).
498 Each boxplot displays the percentage of total mapped small RNAs in each class, with
499 each point representing an individual sample. RNA classes were similarly abundant in
500 both EAD and NF samples, with no statistically significant difference between groups
501 (Wilcoxon test).

502

503

Figure 6

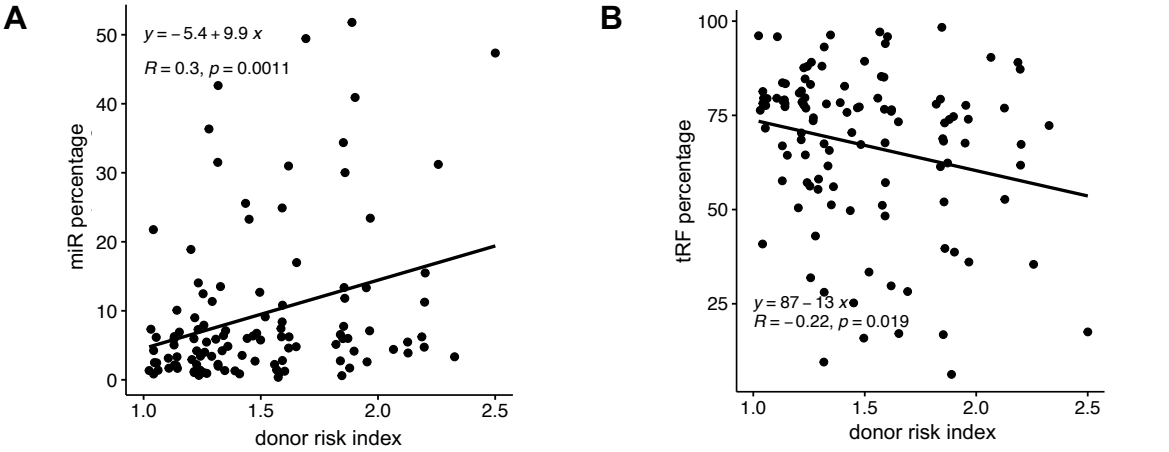
A
y = −5.4 + 9.9 x
R = 0.3, p = 0.0011
miR percentage
donor risk index
B
y = 87 − 13 x
R = −0.22, p = 0.019
tRF percentage
donor risk index

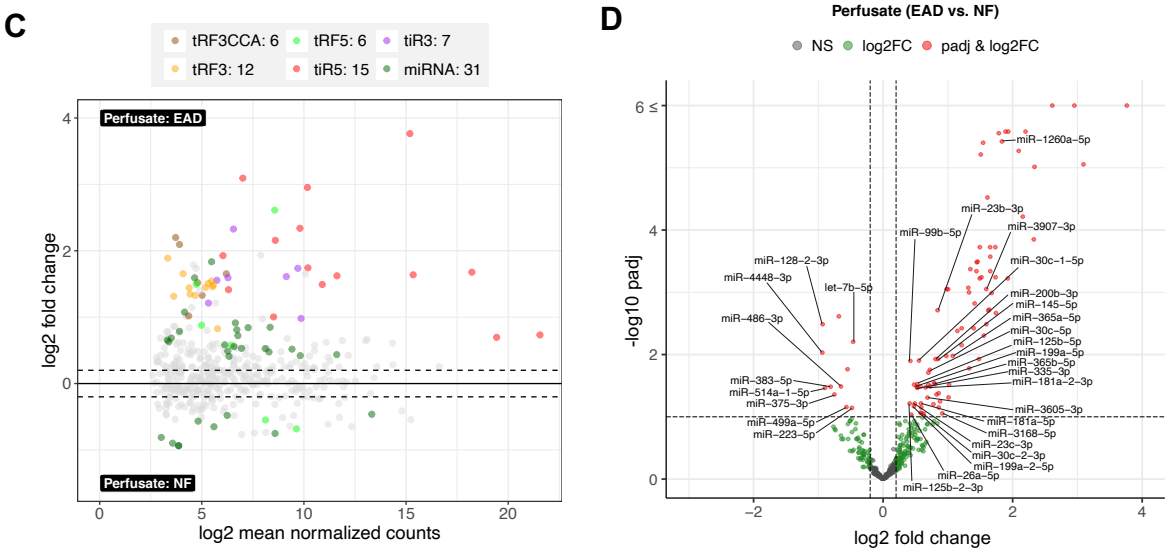
C
tRF3CCA: 6
tRF5: 6
tiR3: 7
tRF3: 12
tiR5: 15
miRNA: 31
Perfusate: EAD
Perfusate: NF
log2 fold change
log2 mean normalized counts
D
Perfusate (EAD vs. NF)
NS
log2FC
padj & log2FC
-log10 padj
log2 fold change
miR−1260a−5p
miR−23b−3p
miR−3907−3p
miR−99b−5p
miR−30c−1−5p
miR−128−2−3p
miR−4448−3p
let−7b−5p
miR−200b−3p
miR−145−5p
miR−365a−5p
miR−486−3p
miR−30c−5p
miR−125b−5p
miR−199a−5p
miR−365b−5p
miR−335−3p
miR−181a−2−3p
miR−383−5p
miR−514a−1−5p
miR−375−3p
miR−3605−3p
miR−181a−5p
miR−499a−5p
miR−3168−5p
miR−223−5p
miR−23c−3p
miR−30c−2−3p
miR−199a−2−5p
miR−26a−5p
miR−125b−2−3p

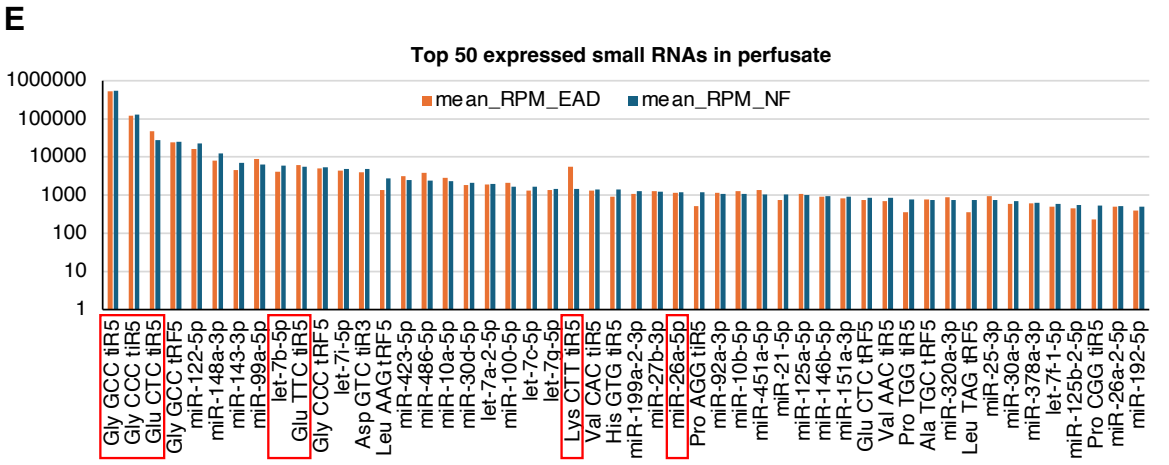
E
Top 50 expressed small RNAs in perfusate
mean_RPM_EAD
mean_RPM_NF
Gly GCC tiR5
Gly CCC tiR5
Glu CTC tiR5
Gly GCC tRF5
miR-122-5p
miR-148a-3p
miR-143-3p
miR-99a-5p
let-7b-5p
Glu TTC tiR5
Gly CCC tRF5
let-7i-5p
Asp GTC tiR3
Leu AAG tRF5
miR-423-5p
miR-486-5p
miR-10a-5p
miR-30d-5p
let-7a-2-5p
miR-100-5p
let-7c-5p
let-7g-5p
Lys CTT tiR5
Val CAC tiR5
His GTG tiR5
miR-199a-2-3p
miR-27b-3p
miR-26a-5p
Pro AGG tiR5
miR-92a-3p
miR-10b-5p
miR-451a-5p
miR-21-5p
miR-125a-5p
miR-146b-5p
miR-151a-3p
Glu CTC tRF5
Val AAC tiR5
Pro TGG tiR5
Ala TGC tRF5
miR-320a-3p
Leu TAG tRF5
miR-25-3p
miR-30a-5p
miR-378a-3p
let-7f-1-5p
miR-125b-2-5p
Pro CGG tiR5
miR-26a-2-5p
miR-192-5p

504 **Figure 6. Pre-transplant perfusate small RNAs are differentially expressed based**
505 **on transplant outcome.**
506 **(A)** Scatter plot depicting the relationship between donor risk index (DRI) and the
507 percentage of small RNA sequencing reads mapped to miRNAs in perfusate samples. A
508 significant positive correlation was observed between miRNA percentage and DRI ($R = 0.30$, $p = 0.0011$). The DRI incorporates donor age, cold ischemia time, cause of death,
510 and race. **(B)** Scatter plot showing the relationship between DRI and the percentage of
511 small RNA sequencing reads mapped to tRFs. A significant negative correlation was
512 observed between DRI and tRF percentage ($R = -0.22$, $p = 0.019$). **(C)** MA plot of the
513 same comparison (EAD vs. NF) in perfusate samples, where the x-axis represents $\log_2$
514 mean normalized counts and the y-axis represents $\log_2$ fold change. Significantly
515 differentially expressed small RNAs (adjusted p-value < 0.1) are color-coded by RNA
516 class (miRNA or tRF subtype). **(D)** Volcano plot showing differential expression of small
517 RNAs in pre-transplant liver perfusate, identified using DESeq2. The x-axis represents
518 $\log_2$ fold change (EAD vs. NF), and the y-axis shows $-\log_{10}$ adjusted p-value. For
519 visualization, all -log10 p-adj values greater than 6 were capped and displayed as 6.
520 Small RNAs meeting significance (adjusted p-value < 0.1) and fold-change thresholds
521 ($|\log_2 FC| \geq 0.2$) are highlighted, while differentially expressed miRNAs labeled**. (E)** Bar
522 plot showing expression levels (mean RPM) of the top fifty most abundant small RNAs
523 detected in liver perfusate samples, stratified by transplant outcome (EAD, orange; NF,
524 blue). Small RNAs that were significantly differentially expressed in EAD vs. NF
525 comparisons are outlined in red.
526

527

Figure 7

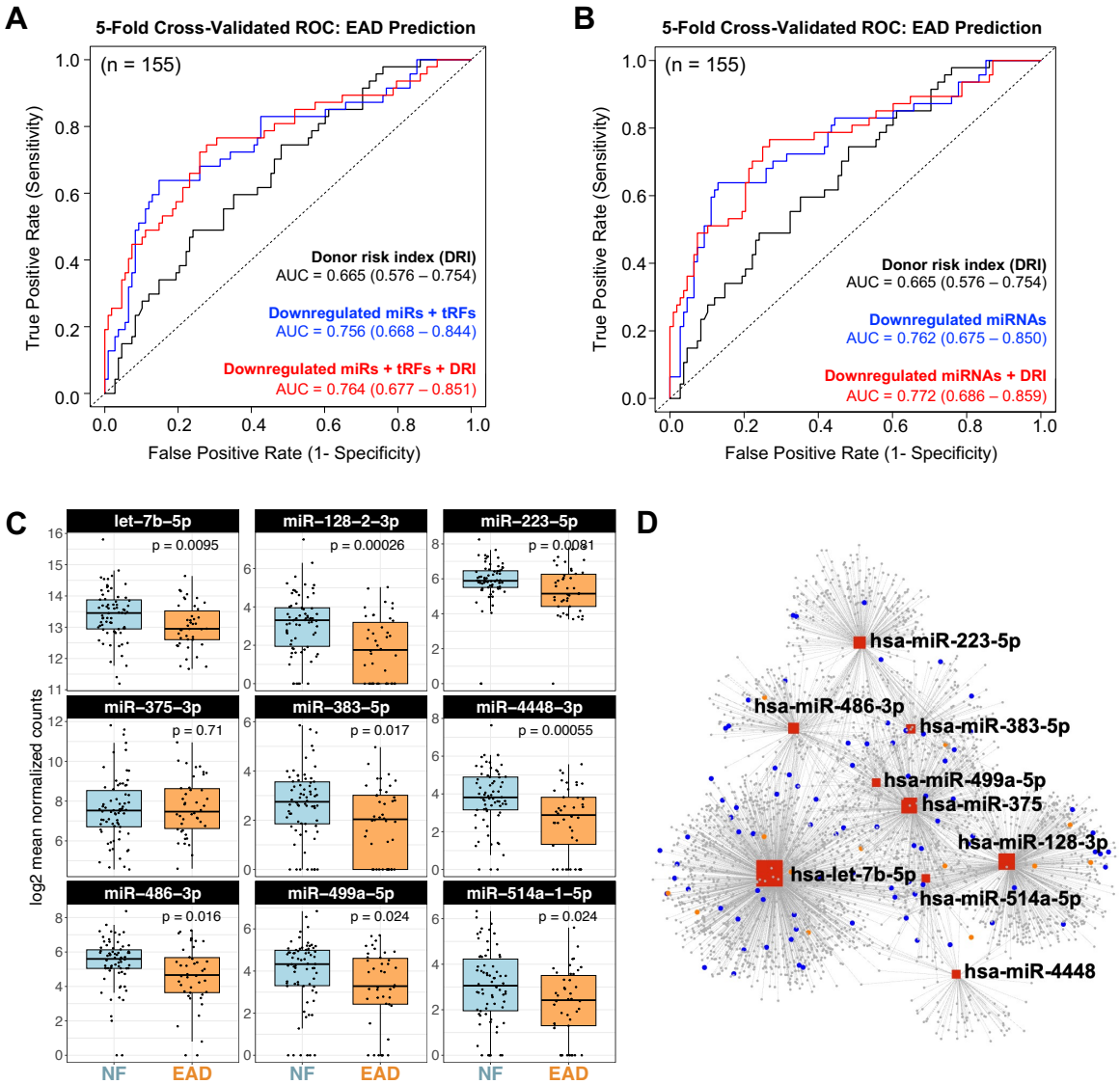

E

Enriched pathways for miR targets (Top 10)

Pathway	Total	Expected	Hits	Pval	FDR
Gene Expression	851	142	219	5.80E-13	6.84E-10
Cellular responses to stress	256	42.9	84	1.03E-10	6.08E-08
SOS-mediated signalling	14	2.34	13	9.09E-10	2.68E-07
GRB2 events in EGFR signaling	14	2.34	13	9.09E-10	2.68E-07
Fc epsilon receptor (FCERI) signaling	169	28.3	60	1.82E-09	4.30E-07
Signaling by Leptin	21	3.52	16	3.05E-09	6.00E-07
SHC1 events in EGFR signaling	15	2.51	13	5.77E-09	9.73E-07
RAF/MAP kinase cascade	10	1.67	10	1.67E-08	2.46E-06
Downstream signal transduction	151	25.3	53	2.56E-08	3.36E-06
Signaling by SCF-KIT	133	22.3	48	4.33E-08	5.11E-06

528 **Figure 7. Downregulated perfusate miRNAs candidates improve EAD prediction.**
529 **(A)** ROC curves comparing three models for predicting EAD: donor risk index (DRI; black),
530 downregulated perfusate tRFs + miRNAs (blue), and a combined model incorporating
531 both perfusate RNAs and DRI (red). The DRI model includes donor age, cold ischemia
532 time, cause of death, and race. The RNA-only model incorporates expression levels of
533 fourteen perfusate RNAs (miRNAs and tRFs) that were significantly downregulated in
534 EAD compared with NF samples. Model performance, assessed by 5-fold cross-
535 validation, yielded AUCs of 0.665 (DRI), 0.756 (downregulated miRNAs + tRFs), and
536 0.764 (combined model). Comparisons using DeLong's test showed no significant
537 differences between the RNA-alone and DRI-alone models (RNA-only vs. DRI, $p = 0.13$),
538 however the combined model (RNAs + DRI) vs. DRI revealed a significant improvement
539 in AUC ($p = 0.047$). **(B)** ROC curves comparing DRI alone (black), downregulated
540 perfusate miRNAs (blue), and a combined miRNA + DRI model (red). The miRNA-only
541 model included nine miRNAs significantly downregulated in EAD perfusate samples
542 relative to NF. The miRNA model outperformed DRI alone (AUC 0.762 vs. 0.665), and
543 the combined model further improved discrimination (AUC 0.772), demonstrating that
544 downregulated perfusate miRNAs add predictive value beyond established donor clinical
545 variables. DeLong's test confirmed the statistically significant difference between the
546 combined model and DRI-only model ($p = 0.033$; miRNA-only vs. DRI, $p = 0.107$). **(C)**
547 Boxplots illustrating the expression of the nine EAD-downregulated perfusate miRNAs
548 used in the ROC analysis (panel B). The y-axis shows $\log_2$ normalized counts, with
549 individual points representing each donor perfusate sample. Reported p-values (Wilcoxon
550 test) reflect significant downregulation of these five miRNAs in EAD relative to NF. **(D)**

551 Network visualization of the nine candidate miRNAs (downregulated in EAD vs. NF),
552 where red squares denote the miRNAs and surrounding circular nodes represent their
553 predicted mRNA targets. Target nodes highlighted in blue correspond to genes belonging
554 to the Reactome pathway, “Cellular responses to stress,” while the nodes highlighted in
555 orange correspond to the top enriched pathway “SOS-mediated signaling.” **(E)** Pathway
556 enrichment results generated from the combined miRNA target set (Reactome database,
557 top 10). For each pathway, the total number of annotated genes, expected overlap,
558 observed hits, p-value, and FDR-adjusted significance are shown.
559

560 **Figure 8**

561

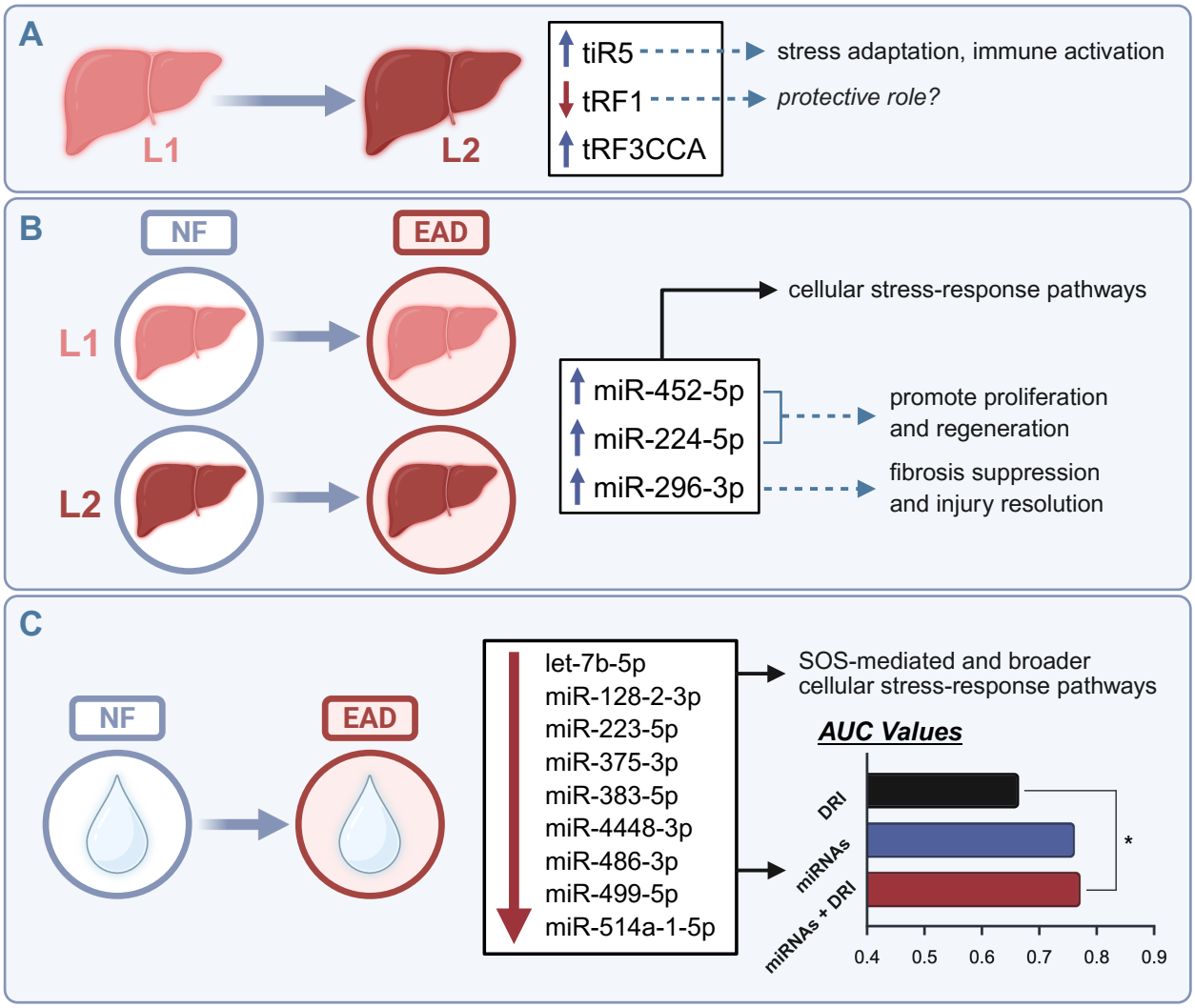

562 **Figure 8. Summary of findings and potential role of tRFs and miRNAs in IRI, EAD**
563 **and clinical outcome.**
564 **A)** Overview of small RNAs differentially expressed in L2 relative to L1 tissue. **B)**
565 Summary of miRNAs and enriched pathways identified in EAD vs NF comparisons across
566 both L1 and L2 tissue. **C)** Summary of nine downregulated perfusate miRNAs with
567 predictive value for EAD and their associated enriched pathways.
568

569 **Methods**

570 Patient recruitment and specimen collection

571 Liver tissue and perfusate samples were obtained from adult orthotopic liver transplant
572 (OLT) recipients (≥18 years old) at Methodist University Hospital after obtaining informed
573 consent. All procedures were conducted under protocols approved by the University of
574 Tennessee Health Science Center Institutional Review Board (IRB#20-07742-XM and
575 IRB#20-07640-XP). Patients were followed for 2 years after transplant. EAD and NF
576 cohorts were defined based on Day 1 AST values based on Olthoff et al EAD definition.
577 Needle biopsy specimens collected pre-implantation (L1) and post-reperfusion (L2) from
578 the same patients were immediately immersed in RNA*later* (Thermo Fisher Scientific, Cat.
579 #AM7021) and incubated at 4 °C overnight to ensure complete permeation. RNA*later* was
580 then removed, and the samples were stored at –80 °C until RNA extraction.

581 Perfusate samples were collected at the end of organ procurement concurrently with pre-
582 implantation liver (L1) biopsies. The solutions were centrifuged at 2,400 rpm for 30
583 minutes at room temperature to remove debris. The resulting supernatant was aliquoted
584 and stored at –80 °C until RNA isolation.

585 Donor livers were transported on ice in the perfusate solution. Average cold ischemia time
586 is 4.5 hours. The perfusate samples were collected in the operation room at the back
587 table before organ was prepped for the transplant and directly placed on ice and
588 transferred to fridge. The perfusate samples were centrifuged and debris was removed.
589 Lastly, the samples were kept at -80°C until RNA isolation. If the perfusate sample had to
590 stay in the fridge overnight and were not centrifuged and frozen on the same they, they
591 were not used in this study.

592

593 RNA isolation and small RNA library preparation

594 Total RNA was extracted from needle biopsies using the Direct-zol RNA MicroPrep Kit
595 (Zymo Research, Cat. #R2062) according to the manufacturer's instructions, including
596 on-column DNase I treatment to remove genomic DNA contamination. For perfusate
597 samples, RNA was isolated from 500 µl of solution using the same kit, following the
598 manufacturer's protocol for liquid samples, and eluted in 15 µl of RNase-free water. RNA
599 concentrations were ranging 50-300 ng/ µl. Purified RNA was stored at –80 °C, and
600 repeated freeze–thaw cycles were avoided to minimize RNA degradation. RNA quality
601 was evaluated using QIAxcel, and each tissue sample exhibited an RNA integrity score
602 (RIS) greater than 6, consistent with high-quality RNA. Perfusate RNA is composed
603 primarily of small RNAs and lacks sufficient intact ribosomal RNA, making it unsuitable
604 for quality assessment using QIAxcel or the Illumina Bioanalyzer. Perfusate RNA
605 concentrations were extremely low and impossible to detect using Qubit RNA HS Assay.
606 Small RNA libraries were prepared using the NEBNext Multiplex Small RNA Library Prep
607 Set for Illumina (New England Biolabs, Cat. #E7330) following the manufacturer's
608 instructions. For each sample, 100 ng of tissue RNA or 5 µl of perfusate RNA was used
609 as input. Indexing was performed using the NEBNext Multiplex Oligos for Illumina, with
610 PCR amplification carried out for 15 cycles for tissue RNA libraries and 18 cycles for
611 perfusate RNA libraries. Amplified products were resolved on an 8% polyacrylamide gel
612 (Thermo Fisher Scientific, Cat. #EC6215BOX), and target bands were excised and
613 purified. Equal amounts of libraries were pooled and sequenced on an Illumina NextSeq
614 500 platform, generating approximately 10 million 75 bp single-end reads per sample.

615 The samples were divided into carefully planned batches. Tissue RNA libraries were
616 prepared in three batches and sequenced in three corresponding batches. For each
617 patient, L1 and L2 samples were always processed within the same batch, and every
618 batch included both EAD and NF samples. Perfusate samples were similarly organized
619 so that each batch contained a mix of EAD and NF samples, minimizing potential batch
620 effects.
621
622 Small RNA-seq data analysis
623 Raw small RNA sequencing reads were trimmed to remove adapter sequences using
624 Cutadapt (v5.1). Adapter-trimmed reads were then mapped and annotated using Unitas
625 (v1.7.3), a specialized tool for comprehensive small RNA annotation similar to previously
626 described (38). Briefly, unitas regular mode allows 1 internal mismatch and maps reads
627 first to human miRbase Release 22 (39), then to other small RNA sequences including
628 genomic tRNA database (40), SILVA rRNA database Release 132 (41) and Ensembl
629 Release 97. In the case of multi-mapping, a read was counted as fraction distributed
630 equally to avoid duplicate counts. For liver biopsy samples, read count matrices
631 generated by Unitas were imported into DESeq2 (v1.44.0) in R for normalization and
632 differential expression analysis. Prior to analysis, RNAs with zero counts in more than 80%
633 of samples were excluded to reduce low-abundance noise. Data visualization was
634 performed in R using ggplot2 (v3.5.1) and ggpubr (v0.6.0). For perfusate samples, read
635 count matrices generated by Unitas were imported into R and normalized using DESEq2
636 with batch correction and DRI in the model. For L2 vs L1 comparisons, DESeq2 design
637 includes patient for paired analysis, all DESeq2 output is included in **Supplementary**

638 **Table 1**. For EAD vs NF comparisons, DESeq2 design includes batch effect and DRI
639 scores, all DESeq2 output is included in **Supplementary Table 2**. The corresponding
640 sample number and significance threshold is indicated in the Figure legends. Data
641 visualization was carried out in R with ggplot2 (v3.5.1) and ggpubr (v0.6.0).
642
643 Clinical correlation and ROC analysis
644 Donor clinical variables were correlated with perfusate small RNA abundance using
645 Pearson correlation in R. Correlation matrices were visualized with the corrplot package
646 (v0.92). Donor Risk Index (DRI) scores were calculated according to the equation defined
647 by Feng et al. (22), which incorporates seven donor or graft characteristics that
648 independently predict graft failure: donor age, donor race, donor height, cause of death,
649 donation after cardiac death, split/partial graft status, and cold ischemia time. ROC curves
650 were generated in R using the ROCR package (v1.0-11). Models were trained using 5-
651 fold cross-validation, in which the dataset was randomly partitioned into five equal subsets;
652 four folds were used to train a logistic model, and the remaining fold served as a held-out
653 test set. This process was repeated five times so that each fold was used once for testing.
654 Reported AUC values represent the mean across give folds. Comparisons between AUCs
655 were performed using DeLong's test in the pROC package (v1.18.5), to assess whether
656 performance differences between models were statistically significant.
657
658 miRNA target prediction and pathway analysis

microRNA target network analysis was performed using miRNet2.0 (42). microRNA targets are predicted by miRTarBase v9.0 (43) and pathway enrichment calculated using hypergeometric test against Reactome pathways (44).

Declarations

Ethics approval and consent to participate

This study was conducted in accordance with the ethical standards of the University of Tennessee Health Science Center Institutional Review Board, which approved all protocols (IRB#20-07742-XM and IRB#20-07640-XP). Liver tissue and perfusate samples were obtained from adult orthotopic liver transplant (OLT) recipients (≥18 years old) at Methodist University Hospital after written informed consent was obtained from all participants.

Availability of data and materials

The small RNA-seq data has been deposited to GEO (GSE311219 and GSE311223).

Competing interests

The authors have no competing interests to declare.

Funding

This research was supported by NIH grants R00CA259526 (to Z.S.), T32NS121721 (to M.A.), T32GM135028 (to K.M.), and Transplant Research Institute at UTHSC start up fund (to C.K.).

682

683 Authors' contributions

684 C.W., G.R., and M.K. helped with patient sample processing, RNA isolation and small
685 RNA library preparation. M.D. and Cem K. coordinated sample collection, storage and
686 contributed to study design. J.E., J.V., and C.E. coordinated patient recruitment and
687 sample collection at the Methodist Hospital. M.A., K.M. and Z.S. performed data analysis
688 on RNA-seq. Canan K. and Z.S. supervised the study and wrote the manuscript with the
689 help of M.A and K.M. All authors read and approved the final manuscript.

690

691 Acknowledgements

692 We would like to thank the Methodist University Hospital transplant team for their
693 assistance with patient recruitment, sample and clinical data collection. We are deeply
694 grateful to the patients and their families for their participation and generous donations to
695 this research. We also would like to acknowledge our colleagues at the Transplant
696 Research Institute for their helpful discussions and ongoing support. We would like to
697 thank IT Research Computing Team at the University of Alabama at Birmingham for NGS
698 support.

699 **References**

700 1. Zhai Y, Petrowsky H, Hong JC, Busuttil RW, Kupiec-Weglinski JW. Ischaemia-
701 reperfusion injury in liver transplantation--from bench to bedside. Nat Rev
702 Gastroenterol Hepatol. 2013 Feb;10(2):79–89.

703 2. Olthoff KM, Kulik L, Samstein B, Kaminski M, Abecassis M, Emond J, et al. Validation
704 of a current definition of early allograft dysfunction in liver transplant recipients and
705 analysis of risk factors. Liver Transpl. 2010 Aug;16(8):943–9.

706 3. Giraudi PJ, Codotto G, Baccarani U, Baralle F, Gondolesi G, Licastro D, et al.
707 Ischemia/Reperfusion Injury and Outcomes in Liver Transplantation Assessed by
708 Omics Technologies: Where Do We Stand? Transplantation. 2025 Aug 13;

709 4. Kumar P, Kuscu C, Dutta A. Biogenesis and Function of Transfer RNA-Related
710 Fragments (tRFs). Trends Biochem Sci. 2016 Aug;41(8):679–89.

711 5. Li G, Manning AC, Bagi A, Yang X, Gokulnath P, Spanos M, et al. Distinct Stress-
712 Dependent Signatures of Cellular and Extracellular tRNA-Derived Small RNAs. Adv
713 Sci (Weinh). 2022 Jun;9(17):e2200829.

714 6. Su Z, Wilson B, Kumar P, Dutta A. Noncanonical Roles of tRNAs: tRNA Fragments
715 and Beyond. Annu Rev Genet. 2020 Nov 23;54:47–69.

716 7. Gebetsberger J, Wyss L, Mleczko AM, Reuther J, Polacek N. A tRNA-derived
717 fragment competes with mRNA for ribosome binding and regulates translation during
718 stress. RNA Biol. 2016 Nov 28;14(10):1364–73.

719 8. Emara MM, Ivanov P, Hickman T, Dawra N, Tisdale S, Kedersha N, et al. Angiogenin-
720 induced tRNA-derived Stress-induced RNAs Promote Stress-induced Stress Granule
721 Assembly. J Biol Chem. 2010 Apr 2;285(14):10959–68.

722 9. Goodarzi H, Liu X, Nguyen HCB, Zhang S, Fish L, Tavazoie SF. Endogenous tRNA-
723 Derived Fragments Suppress Breast Cancer Progression via YBX1 Displacement.
724 Cell. 2015 May 7;161(4):790–802.

725 10. Kuscu C, Kumar P, Kiran M, Su Z, Malik A, Dutta A. tRNA fragments (tRFs) guide Ago
726 to regulate gene expression post-transcriptionally in a Dicer-independent manner.
727 RNA. 2018 Aug;24(8):1093–105.

728 11. Li G, Sun L, Xin C, Hao T, Kharel P, Manning AC, et al. A hypoxia-responsive tRNA-
729 derived small RNA confers renal protection through RNA autophagy. Science. 2025
730 Aug 28;389(6763):eadp5384.

731 12. Anderson P, Ivanov P. tRNA fragments in human health and disease. FEBS Lett.
732 2014 Nov 28;588(23):4297–304.

733 13. Pandey KK, Madhry D, Ravi Kumar YS, Malvankar S, Sapra L, Srivastava RK, et al.
734 Regulatory roles of tRNA-derived RNA fragments in human pathophysiology. Mol
735 Ther Nucleic Acids. 2021 Dec 3;26:161–73.

736 14. Costa B, Li Calzi M, Castellano M, Blanco V, Cuevasanta E, Litvan I, et al. Nicked
737 tRNAs are stable reservoirs of tRNA halves in cells and biofluids. Proc Natl Acad Sci
738 U S A. 2023 Jan 24;120(4):e2216330120.

739 15. Srinivasan S, Yeri A, Cheah PS, Chung A, Danielson K, De Hoff P, et al. Small RNA
740 Sequencing across Diverse Biofluids Identifies Optimal Methods for exRNA Isolation.
741 Cell. 2019 Apr 4;177(2):446-462.e16.

742 16. Mas VR, Dumur CI, Scian MJ, Gehrau RC, Maluf DG. MicroRNAs as biomarkers in
743 solid organ transplantation. Am J Transplant. 2013 Jan;13(1):11–9.

744 17. van de Vrie M, Deegens JK, Eikmans M, van der Vlag J, Hilbrands LB. Urinary
745 MicroRNA as Biomarker in Renal Transplantation. Am J Transplant. 2017
746 May;17(5):1160–6.

747 18. Koch PF, Ludwig K, Krenzien F, Hillebrandt KH, Schöning W, Pratschke J, et al.
748 miRNA as potential biomarkers after liver transplantation: A systematic review.
749 Transplant Rev (Orlando). 2024 Apr;38(2):100831.

750 19. Farid WRR, Pan Q, van der Meer AJP, de Ruiter PE, Ramakrishnaiah V, de Jonge J,
751 et al. Hepatocyte-derived microRNAs as serum biomarkers of hepatic injury and
752 rejection after liver transplantation. Liver Transpl. 2012 Mar;18(3):290–7.

753 20. Khorsandi SE, Quaglia A, Salehi S, Jassem W, Vilca-Melendez H, Prachalias A, et al.
754 The microRNA Expression Profile in Donation after Cardiac Death (DCD) Livers and
755 Its Ability to Identify Primary Non Function. PLOS ONE. 2015 May 15;10(5):e0127073.

756 21. Matton APM, Selten JW, Roest HP, de Jonge J, IJzermans JNM, de Meijer VE, et al.
757 Cell-free microRNAs as early predictors of graft viability during ex vivo normothermic
758 machine perfusion of human donor livers. Clin Transplant. 2020 Mar;34(3):e13790.

759 22. Feng S, Goodrich NP, Bragg-Gresham JL, Dykstra DM, Punch JD, DebRoy MA, et al.
760 Characteristics associated with liver graft failure: the concept of a donor risk index.
761 Am J Transplant. 2006 Apr;6(4):783–90.

762 23. Ivanov P, Emara MM, Villen J, Gygi SP, Anderson P. Angiogenin-induced tRNA
763 fragments inhibit translation initiation. Mol Cell. 2011 Aug 19;43(4):613–23.

764 24. Pawar K, Kawamura T, Kirino Y. The tRNAVal half: A strong endogenous Toll-like
765 receptor 7 ligand with a 5'-terminal universal sequence signature. Proc Natl Acad Sci
766 U S A. 2024 May 7;121(19):e2319569121.

767 25. Pawar K, Shigematsu M, Sharbati S, Kirino Y. Infection-induced 5′-half molecules of
768 tRNAHisGUG activate Toll-like receptor 7. PLOS Biology. 2020 Dec
769 17;18(12):e3000982.

770 26. Yu J, Zhang X, Cai C, Zhou T, Chen Q. Small RNA and Toll-like receptor interactions:
771 origins and disease mechanisms. Trends Biochem Sci. 2025 May;50(5):385–401.

772 27. Rong MH, Cai KT, Lu HP, Guo YN, Huang XY, Zhu ZH, et al. Overexpression of MiR-
773 452-5p in hepatocellular carcinoma tissues and its prospective signaling pathways.
774 Int J Clin Exp Pathol. 2019 Nov 1;12(11):4041–56.

775 28. Li A, Wu N, Sun J. E2F1-induced microRNA-224-5p expression is associated with
776 hepatocellular carcinoma cell migration, invasion and epithelial-mesenchymal
777 transition via MREG. Oncol Lett. 2022 Mar;23(3):82.

778 29. Markovic J, Li R, Khanal R, Peng Q, Möbus S, Yuan Q, et al. Identification and
779 functional validation of miR-190b-5p and miR-296-3p as novel therapeutic attenuators
780 of liver fibrosis. J Hepatol. 2025 Feb;82(2):301–14.

781 30. Darden CM, Saracino G, Otajonova N, Vasu S, Wang X, Onaca N, et al. Exosomal
782 Small RNA From Donor Liver Preservation Solution Exhibits Molecular Signatures
783 That Distinguish Organ Quality and Posttransplant Complications. Transplant Direct.
784 2025 Sep 18;11(10):e1847.

785 31. Zhang C, Sun C, Zhao Y, Ye B, Yu G. Signaling pathways of liver regeneration:
786 Biological mechanisms and implications. iScience. 2024 Jan 19;27(1):108683.

787 32. Liang J, Li A, Chen J, Cao N, Zhu T, Cai R, et al. MicroRNA Let-7b-5p Targets IGF1R
788 to Inhibit the Progression of Hepatocellular Carcinoma Through the AKT/mTOR
789 Pathway. Cancer Med. 2025 Jun;14(12):e71000.

790 33. Zhou C, Chen Z, Peng C, Chen C, Li H. Long Noncoding RNA TRIM52-AS1 Sponges
791 miR-514a-5p to Facilitate Hepatocellular Carcinoma Progression Through Increasing
792 MRPS18A. Cancer Biother Radiopharm. 2021 Mar;36(2):211–9.

793 34. Mou T, Luo Y, Huang Z, Zheng D, Pu X, Shen A, et al. Inhibition of microRNA-128-3p
794 alleviates liver ischaemia-reperfusion injury in mice through repressing the Rnd3/NF-
795 κB axis. Innate Immun. 2020 Aug;26(6):528–36.

796 35. Kellner MJ, Koob JG, Gootenberg JS, Abudayyeh OO, Zhang F. SHERLOCK: nucleic
797 acid detection with CRISPR nucleases. Nat Protoc. 2019 Oct;14(10):2986–3012.

798 36. Zhao S, Zhang Q, Luo R, Sun J, Zhu C, Zhou D, et al. Amplification-free miRNA
799 detection with CRISPR/Cas12a system based on fragment complementary activation
800 strategy. Chem Sci. 2024 Oct 17;15(44):18347–54.

801 37. De Silva PIT, Hiniduma K, Canete R, Bhalerao KS, Shawky SM, Gunathilaka H, et al.
802 Multiplexed CRISPR Assay for Amplification-Free Detection of miRNAs. Biosensors
803 (Basel). 2025 May 29;15(6):346.

804 38. Su Z, Monshaugen I, Wilson B, Wang F, Klungland A, Ougland R, et al. TRMT6/61A-
805 dependent base methylation of tRNA-derived fragments regulates gene-silencing
806 activity and the unfolded protein response in bladder cancer. Nat Commun. 2022 Apr
807 20;13(1):2165.

808 39. Kozomara A, Birgaoanu M, Griffiths-Jones S. miRBase: from microRNA sequences
809 to function. Nucleic Acids Res. 2019 Jan 8;47(D1):D155–62.

810 40. Chan PP, Lowe TM. GtRNAdb 2.0: an expanded database of transfer RNA genes
811 identified in complete and draft genomes. Nucleic Acids Res. 2016 Jan
812 4;44(D1):D184-189.

813 41. Quast C, Pruesse E, Yilmaz P, Gerken J, Schweer T, Yarza P, et al. The SILVA
814 ribosomal RNA gene database project: improved data processing and web-based
815 tools. Nucleic Acids Res. 2013 Jan;41(Database issue):D590-596.

816 42. Chang L, Zhou G, Soufan O, Xia J. miRNet 2.0: network-based visual analytics for
817 miRNA functional analysis and systems biology. Nucleic Acids Res. 2020 Jul
818 2;48(W1):W244–51.

819 43. Skoufos G, Kakoulidis P, Tastsoglou S, Zacharopoulou E, Kotsira V, Miliotis M, et al.
820 TarBase-v9.0 extends experimentally supported miRNA–gene interactions to cell-
821 types and virally encoded miRNAs. Nucleic Acids Res. 2024 Jan 5;52(D1):D304–10.

822 44. Milacic M, Beavers D, Conley P, Gong C, Gillespie M, Griss J, et al. The Reactome
823 Pathway Knowledgebase 2024. Nucleic Acids Res. 2024 Jan 5;52(D1):D672–8.

824